High-Efficiency Solution-Processed Inorganic Metal Halide Perovskite Light-Emitting Diodes

*Himchan Cho, Christoph Wolf, Joo Sung Kim, Hyung Joong Yun, Jong Seong Bae, Hobeom Kim, Jung-Min Heo, Soyeong Ahn, and Tae-Woo Lee**

This paper reports highly bright and efficient $CsPbBr_3$ perovskite light-emitting diodes (PeLEDs) fabricated by simple one-step spin-coating of uniform $CsPbBr_3$ polycrystalline layers on a self-organized buffer hole injection layer and stoichiometry-controlled $CsPbBr_3$ precursor solutions with an optimized concentration. The PeLEDs have maximum current efficiency of 5.39 cd A^{-1} and maximum luminance of 13752 cd m^{-2}. This paper also investigates the origin of current hysteresis, which can be ascribed to migration of Br^- anions. Temperature dependence of the electroluminescence (EL) spectrum is measured and the origins of decreased spectrum area, spectral blue-shift, and linewidth broadening are analyzed systematically with the activation energies, and are related with Br^- anion migration, thermal dissociation of excitons, thermal expansion, and electron–phonon interaction. This work provides simple ways to improve the efficiency and brightness of all-inorganic polycrystalline PeLEDs and improves understanding of temperature-dependent ion migration and EL properties in inorganic PeLEDs.

Metal halide perovskites (MHPs) have recently attracted much attention of researchers in field of optoelectronics including light-emitting diodes.[1–4] MHPs have been used as emission layers in perovskite light-emitting diodes (PeLEDs), and have many advantages such as high charge-carrier mobility, solution processability, high color purity, color tunability, and low material cost.[1,2,5–11] Especially, PeLEDs that use methylammonium lead bromide ($MAPbBr_3$) emission layers showed a breakthrough in external quantum efficiency (EQE) of green PeLEDs (8.53%) and demonstrated that PeLEDs can be competitive with organic LEDs and quantum dot (QD) LEDs.[2] In addition to the visible PeLEDs, recent publications in infrared PeLEDs demonstrated EQE up to 8.8%[12] and 11.7%.[13]

Despite the outstanding increase in EQE, the chemical instability of MA cations can cause PeLEDs to be unstable in the presence of light, moisture and heat.[14] To overcome these problems, all-inorganic MHPs such as cesium lead halides ($CsPbX_3$) have been evaluated.[15–27] $CsPbX_3$ has much higher thermal decomposition temperature (≈580 °C for $CsPbBr_3$) than does $MAPbBr_3$ (≈220 °C).[12] Also, $CsPbBr_3$ has very high photoluminescence (PL) quantum efficiency up to 90%,[15,17] with narrower PL spectrum (full width at half maximum, FWHM = 17–19 nm)[15,17,18,20,22,23] than $MAPbBr_3$ (FWHM ≈ 20 nm).[2] To exploit these advantages, many approaches have been studied to fabricate PeLEDs based on $CsPbBr_3$.[18–27] Most studies used the synthesis of colloidal $CsPbBr_3$ QDs to improve the luminescent property of $CsPbBr_3$ by exploiting the quantum size effect,[19–25] but these methods require careful synthesis process and insulating organic ligands around QDs hamper the charge injection into the QD and transport through the films. Furthermore, the increased number of surface defects on the $CsPbBr_3$ QDs can also hamper electroluminescence (EL) efficiency. On the other hand, PeLEDs based on $CsPbBr_3$ polycrystalline films can be much more simple to fabricate because the $CsPbBr_3$ polycrystalline films can be formed by using a simple one-step spin-coating, which can potentially avoid the problems that exist in perovskite QD LEDs.[18,26,27] Bright polycrystalline $CsPbBr_3$ PeLEDs have been achieved by adding excess CsBr to $CsPbBr_3$ precursor solutions (luminance = 407 cd m^{-2}[18] and 7276 cd

Dr. H. Cho, J. S. Kim, J.-M. Heo, Prof. T.-W. Lee
Department of Materials Science and Engineering
Seoul National University
1 Gwanak-ro, Gwanak-gu, Seoul 08826, Republic of Korea
E-mail: twlees@snu.ac.kr, taewlees@gmail.com
Dr. H. Cho, Prof. T.-W. Lee
Research Institute of Advanced Materials
Seoul National University
1 Gwanak-ro, Gwanak-gu, Seoul 08826, Republic of Korea
Dr. H. Cho, Prof. T.-W. Lee
BK21 PLUS SNU Materials Division for
Educating Creative Global Leaders
Seoul National University
1 Gwanak-ro, Gwanak-gu, Seoul 08826, Republic of Korea
C. Wolf, H. Kim, S. Ahn
Department of Materials Science and Engineering
Pohang University of Science and Technology (POSTECH)
77 Cheongam-ro, Nam-gu, Pohang, Gyungbuk 37673, Republic of Korea
Dr. H. J. Yun
Advance Nano Research Group
Korea Basic Science Institute (KBSI)
169-148 Gwahak-ro, Yuseong-gu, Daejeon 34133, Republic of Korea
Dr. J. S. Bae
Division of Analysis and Research
Korea Basic Science Institute (KBSI)
618-230 Gwahaksandan 1-ro, Gangseo-gu, Busan 46742, Republic of Korea

DOI: 10.1002/adma.201700579

m^{-2},[27] EQE = 0.008%[18] and 0.15%[27]) and by mixing poly(ethylene oxide) with $CsPbBr_3$ precursor solutions (luminance = 53525 cd m^{-2} and EQE = 4.26%).[26] However, one-step spin-coating of inorganic $CsPbBr_3$ precursor solutions without any host materials had difficulty in forming uniform pure $CsPbBr_3$ polycrystalline layers.[18] Furthermore, the EL efficiencies of pure polycrystalline-$CsPbBr_3$ PeLEDs[18,27] are still much lower (EQE = 0.008%–0.15%) than that of organic–inorganic hybrid $MAPbBr_3$ PeLEDs (EQE = 8.53%);[2] therefore, effective ways to further increase EL efficiency of inorganic $CsPbBr_3$ PeLEDs must be explored.

To establish an effective research strategy for PeLEDs, in-depth understanding of fundamental ionic and electronic properties of MHPs including ion migration, nonradiative recombination/relaxation processes, and electron–phonon interaction are also imperative in addition to the development of processes and device engineering to boost up the EL efficiency. Ion migration and concomitant formation of charge carrier traps are considered to be the origins of the unusual optical and electronic behaviors of MHPs, such as current hysteresis,[28] PL increase by continuous photoexcitation,[29] fluorescence blinking,[30] and bias-induced PL quenching.[31] Therefore, ion migration in MHPs is thought to have a very close relationship with EL in PeLEDs. Also, understanding of nonradiative pathways can help to find a way to minimize EL quenching. Furthermore, electron–phonon interaction has strong influences on EL properties such as bandgap and linewidth broadening.[32–35] For these purposes, ion migration in MHPs has been studied theoretically[36–38] and experimentally,[39,40] and the nonradiative pathways and the electron–phonon interaction in $CsPbBr_3$ have been investigated based on temperature-dependent PL analysis.[32–35] However, ion migration has not been investigated in $CsPbBr_3$ PeLEDs. Also, the thermal deactivation pathways of EL and the influence of electron–phonon interaction on EL properties in PeLEDs have not been studied. Furthermore, previous studies focused on $CsPbBr_3$ QDs, not on $CsPbBr_3$ bulk polycrystalline films.

In this work, we achieved high-efficiency polycrystalline $CsPbBr_3$ PeLEDs (**Figure 1**a) by a simple spin-coating without (i) complex QD synthesis and (ii) incorporating a host material, and performed a systematic temperature-dependent analysis to understand ion migration, EL deactivation and electron–phonon interaction in $CsPbBr_3$ PeLEDs. High-efficiency polycrystalline $CsPbBr_3$ PeLEDs with maximum current efficiency (CE) of 5.39 cd A^{-1} and maximum luminance of 13752 cd m^{-2} were achieved by using completely uniform pure $CsPbBr_3$ polycrystalline layers fabricated on a self-organized buffer hole injection layer (Buf-HIL), and by controlling stoichiometry of $CsPbBr_3$ precursor solutions to prevent EL quenching. Current hysteresis occurred at all temperatures and increased exponentially as T increased; this trend can be ascribed to migration of Br^- anions. We also observed the temperature dependence of EL spectrum; the activation energies for EL quenching, blueshift and linewidth broadening were obtained and the origins of changes were analyzed. This work provides methods to increase the efficiency of $CsPbBr_3$ PeLEDs, and increases understanding of ion migration, EL deactivation pathways, and electron–phonon interaction in $CsPbBr_3$ layers in the PeLEDs.

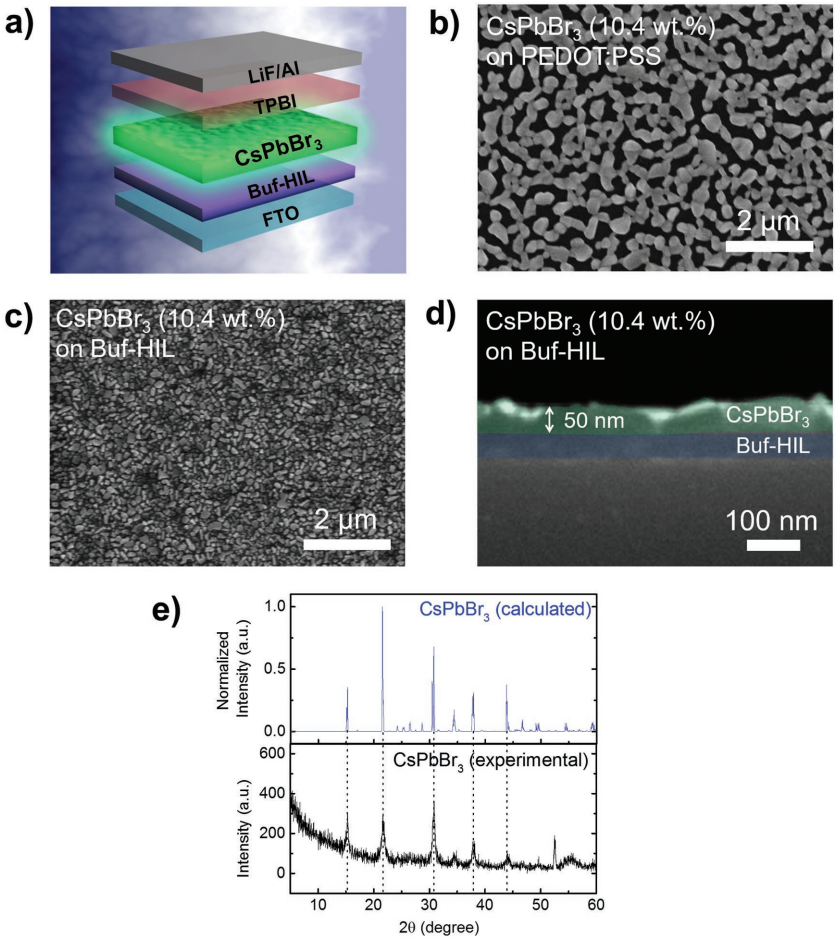

Figure 1. a) Schematic $CsPbBr_3$ PeLED structure. Scanning electron microscope (SEM) images of $CsPbBr_3$ films of 10.4 wt% b) on a PEDOT:PSS layer and c) on a Buf-HIL. d) SEM image of cross-section of 10.4 wt% $CsPbBr_3$ films. e) Measured XRD pattern of a $CsPbBr_3$ film of 10.4 wt% (black) and calculated pattern of orthorhombic $CsPbBr_3$ (blue).[42]

To fabricate uniform $CsPbBr_3$ polycrystalline films, we used two approaches: use of Buf-HIL as underlying layers; and optimization of precursor concentration. We prepared $CsPbBr_3$ polycrystalline films by spin-coating $CsPbBr_3$ precursor solutions on silicon wafer/poly(3,4-ethylenedioxythiophene):polystyrene sulfonate (PEDOT:PSS) or Buf-HIL (a mixture of PEDOT, PSS, and perfluorinated ionomer (PFI) at weight ratio of PEDOT:PSS:PFI = 1:6:25.4).[5] On PEDOT:PSS, $CsPbBr_3$ films were not uniform and the grains were not closely packed, so much of the PEDOT:PSS surface was not covered (Figure 1b). Use of Buf-HIL instead of PEDOT:PSS yielded

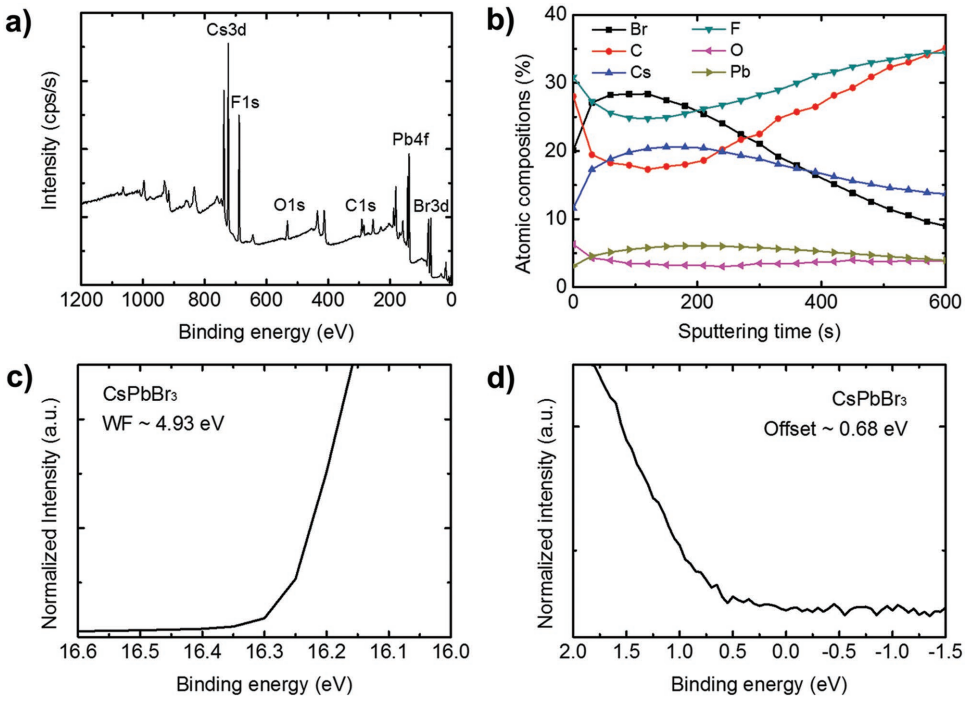

Figure 2. a) XPS survey spectrum and b) depth profiling of a $CsPbBr_3$ film. UPS spectra of a $CsPbBr_3$ film c) showing the secondary cut-off and d) the offset between WF and IE of $CsPbBr_3$ ($CsBr:PbBr_2$ = 1.1:1, mol:mol).

uniform $CsPbBr_3$ films with full coverage and closely packed grains (Figure 1c). The formation of uniform $CsPbBr_3$ films on Buf-HIL may be attributed to the slight dissolution of PFI into $CsPbBr_3$ solution loaded on Buf-HIL, and to reduction of grain size as a consequence of PFI chains impeding crystal growth. We also considered that the copious branching of dissolved PFI molecules (Figure S1, Supporting Information) may facilitate heterogeneous nucleation[41] and increase the number of nucleation sites.

The concentration of $CsPbBr_3$ precursor solution was optimized to fabricate uniform $CsPbBr_3$ films. Solutions of 7.5, 9.0, and 10.4 wt% $CsPbBr_3$ in dimethyl sulfoxide (DMSO) were prepared, and the morphologies of the resulting films were compared (Figure 1c ; Figure S2, Supporting Information). Uniform full-coverage $CsPbBr_3$ films were obtained only by using 10.4 wt% solutions (Figure 1c); concentrations <10.4 wt% included an insufficient amount of precursor, so the PEDOT:PSS layers were not fully covered (Figure S2, Supporting Information). This non-uniformity allows formation of electrical shunt paths, which decrease EL efficiency.[2] The $CsPbBr_3$ film (10.4 wt%) was ≈50 nm thick (Figure 1d).

To study the crystal structure of the prepared pure $CsPbBr_3$ polycrystalline film, its X-ray diffraction (XRD) pattern was measured (Figure 1e). The pattern had distinctive peaks at ≈15.32°, ≈21.66°, ≈30.86°, and ≈38.04° which can be assigned to (101), (121), (202), and (321) planes, respectively.[18] The peak positions were in complete correspondence with those of calculated orthorhombic $CsPbBr_3$ XRD patterns based on a previous report;[42] these results demonstrate that $CsPbBr_3$ had the orthorhombic *Pnma* phase.

Surface bonding states of the $CsPbBr_3$ films ($CsBr:PbBr_2$ = 1.1:1) were analyzed using X-ray photoelectron spectroscopy (XPS). The survey spectrum exhibited distinctive peaks of Cs, Pb, and Br; which confirm the presence of $CsPbBr_3$ (**Figure 2**a). The detailed chemical bonding status at the surface of $CsPbBr_3$ films was analyzed by deconvoluting XPS peaks (Figure S3, Supporting Information). In the Pb4f spectrum, only $Pb4f_{7/2}$ (138.80 eV) and $Pb4f_{5/2}$ (143.65 eV) peaks were observed (Figure S3a, Supporting Information); peaks of metallic Pb were absent.[2,43] The emergence of metallic Pb was prevented by increasing CsBr molar proportion by 10 mol%.[2] $Cs3d_{5/2}$ (725.20 eV) and $Cs3d_{3/2}$ (739.15 eV) peaks were observed in the Cs3d spectrum, and $Br3d_{5/2}$ (68.70 eV) and $Br3d_{3/2}$ (69.70 eV) peaks were observed in Br3d spectrum;[43] these results confirm the existence of Cs and Br species at the surface (Figure S3b,c, Supporting Information). The peak positions in Pb4f and Br3d were very similar to a previous report.[2]

The presence of PFI was confirmed by F1s and C1s spectra (Figure S3d,e, Supporting Information). The peaks at 689.90 eV can be assigned to C—F* bonds, and in the C1s spectrum, the peaks at 285.65, 290.50, 292.60, and 294.20 eV correspond to C—C (sp^3, hydrocarbon contamination), $-CF_2^-$, $-OCFSO_2^-$, and $-CF_3$ bonds, respectively; these positions matched well with previously reported XPS characteristics of PFI membrane.[44]

The emergence of strong F1s peak that originated from PFI indicates the possibilities: (1) that the $CsPbBr_3$ films still had small voids along grain boundaries, and (2) that the PFI-rich surface of the underlying Buf-HIL had partially dissolved into the $CsPbBr_3$ solutions during spin-coating. In the latter case, PFI chains can be located between $CsPbBr_3$ grains or even on them.

To clarify the distribution of PFI, the vertical distribution of chemical species inside the $CsPbBr_3$ film was characterized by

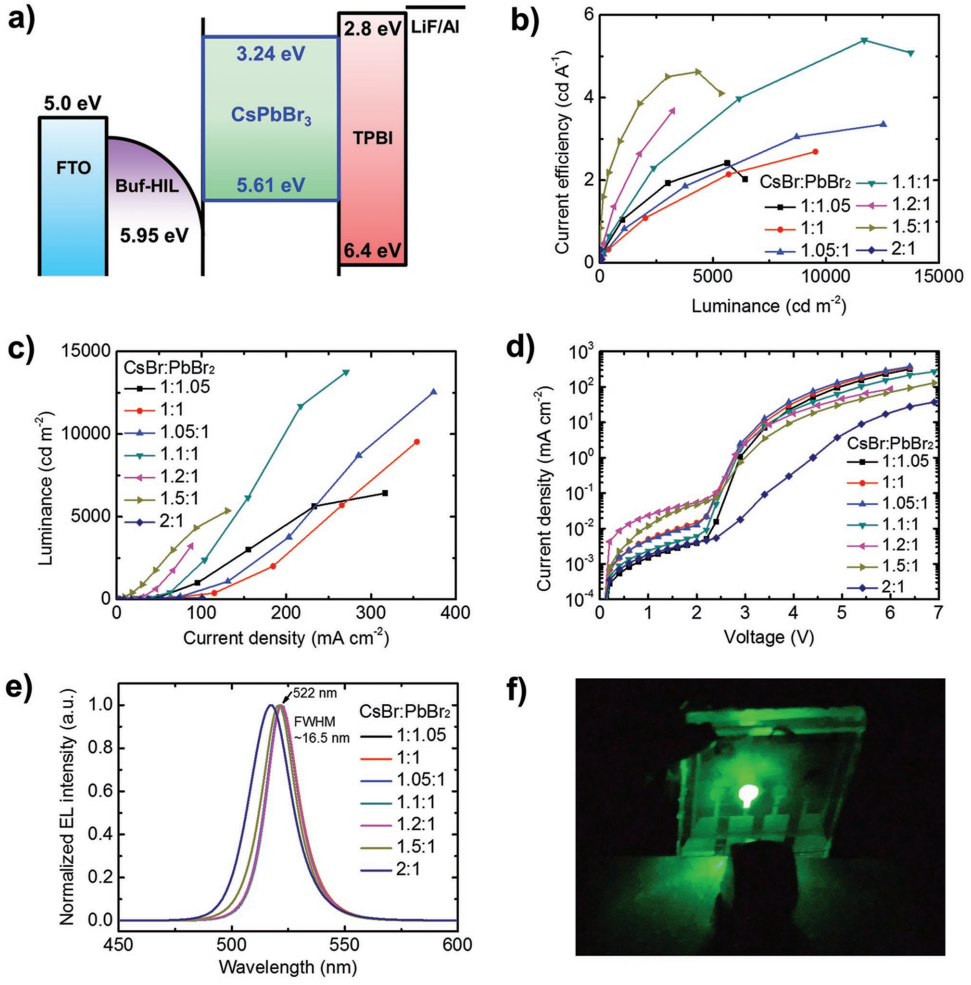

Figure 3. a) Energy level diagram of $CsPbBr_3$ PeLEDs. b) CE, c) luminance, d) current density, and e) EL spectra of $CsPbBr_3$ PeLEDs with varying molar ratio $CsBr:PbBr_2$. f) Photograph of $CsPbBr_3$ PeLED during operation.

conducting XPS depth profiling (Figure 2b). The use of an Ar gas cluster ion beam avoided possible beam damage to $CsPbBr_3$ films. The compositions of C and F were dominant at the surface, decreased until sputtering time of 120 s, then increased at longer times (Figure 2b). The gradual increases in C and F compositions after 120 s suggest that those compositions were related to the underlying PFI-rich surface of Buf-HIL that had a gradient PFI profile.[5] While C and F compositions decreased, the proportions of Cs and Br increased. These gradual antiparallel trends in the atomic compositions confirm the presence of PFI between or even on the $CsPbBr_3$ grains, and verify the partial dissolution of PFI into the $CsPbBr_3$ solutions loaded on the Buf-HIL during spin-coating. Because of the gradually increasing composition of PFI, which has a high ionization energy,[45,46] Buf-HIL can reduce the hole injection barrier with increased work function (WF), and suppress exciton quenching at the Buf-HIL/$CsPbBr_3$ interfaces.[5] Therefore, the presence of PFI between or on the $CsPbBr_3$ grains may increase the interfacial area, and thereby further enhance hole injection and further suppress exciton quenching.

To construct an energy-level diagram of the PeLED structure (Figure 1a), WF and ionization energy (IE) of $CsPbBr_3$ layers were measured using ultraviolet photoelectron spectroscopy (UPS) (Figure 2c,d). WF was calculated to be ≈4.93 eV (Figure 2c) from the intersection point of two tangents at the secondary cut-off region. The energy offset between WF and IE was calculated as ≈0.68 eV; i.e., IE ≈ 5.61 eV,[2] which is consistent with previous reports that $CsPbBr_3$ has $5.5 \leq IE \leq 6.18$ eV.[16,18,20,21]

Using the uniform $CsPbBr_3$ polycrystalline layers as emission layers, PeLEDs were fabricated with the structure of fluorine doped tin oxide (FTO)/Buf-HIL/$CsPbBr_3$/1,3,5-tris(*N*-phenylbenzimidazol-2-yl)benzene (TPBI) (50 nm)/LiF (1 nm)/Al (100 nm) (Figure 1a). The energy level diagram (**Figure 3**a) was drawn based on the obtained IE of $CsPbBr_3$ (Figure 2c,d) and a previous report.[2] To increase the efficiency of PeLEDs, the stoichiometry control of $CsPbBr_3$ precursor solutions was used.[2] The PeLEDs that used $CsPbBr_3$ layers with $CsBr:PbBr_2$ = 1.1:1 showed the highest maximum CE = 5.39 cd A^{-1} (EQE = 1.37%) and the highest maximum luminance = 13752 cd m^{-2}, while showing similar current density to those of PeLEDs with $CsBr:PbBr_2$ = 1.05:1, 1:1, and 1:1.05 (Figure 3b–d). To the best of our knowledge, this is the highest reported efficiency for PeLEDs based on pure $CsPbBr_3$ polycrystalline emission layers.

Table 1. Maximum CE (cd A^{-1}) and luminance (cd m^{-2}) of $CsPbBr_3$ PeLEDs depending on the molar ratio $CsBr:PbBr_2$.

$CsBr:PbBr_2$	Max. CE	Max. luminance
1:1.05	2.42	6425
1:1	2.69	9539
1.05:1	3.35	12538
1.1:1	5.39	13752
1.2:1	3.68	3226
1.5:1	4.63	5362
2:1	0.0976	82

The gradual increase in CsBr molar ratio from $CsBr:PbBr_2$ = 1:1.05 to $CsBr:PbBr_2$ = 1.1:1 resulted in gradual increases in maximum CE and luminance (Figure 3b,c and **Table 1**; Figure S4, Supporting Information); these trends can be attributed to the removal of metallic Pb.[2] The absence of metallic Pb greatly helps to increase luminescence efficiency of $CsPbBr_3$ films by preventing luminescence quenching.[2] As CsBr molar ratio was further increased from $CsBr:PbBr_2$ = 1.1:1, the current density tended to decrease due to insulating CsBr remnants and the maximum luminance also decreased because the devices could not withstand high electric fields. The maximum CE also decreased accordingly. However, the CE at low luminance <3000 cd m^{-2} was the highest at $CsBr:PbBr_2$ = 1.5:1 due to the improved balance of electron and holes (Figure 3b–d and Table 1; Figure S4, Supporting Information). Compared with the $CsPbBr_3$ PeLEDs based on Buf-HIL, $CsPbBr_3$ PeLEDs based on PEDOT:PSS exhibited poor CE and luminance (0.815 cd A^{-1} and 2328 cd m^{-2}, respectively) due to the high leakage current (Figure S5, Supporting Information). The $CsPbBr_3$ PeLEDs exhibited very narrow EL spectra with FWHM of 16.5 nm (Figure 3e), which is much smaller than those of organic LEDs (≈40 nm) and QD LEDs (≈30 nm) and even smaller than those of $MAPbBr_3$ PeLEDs (≈20 nm).[2] We tested the device operational lifetime of $CsPbBr_3$ PeLEDs in comparison with $MAPbBr_3$ and $FAPbBr_3$ PeLEDs based on the same device structure (Figure S6, Supporting Information). The operating voltage shift is the most stable in the $CsPbBr_3$ PeLED (≈0.033 V min^{-1}) compared with those in the $MAPbBr_3$ PeLED (≈0.046 V min^{-1}) and $FAPbBr_3$ PeLED (≈0.42 V min^{-1}). The luminance decay of $CsPbBr_3$ PeLED was slower than that of $FAPbBr_3$ PeLED and faster than that of $MAPbBr_3$ PeLED. This fast luminance decay can be ascribed to the poor film morphology of thin $CsPbBr_3$ layers (≈50 nm) with large voids at the grain boundaries that facilitate the formation of shunting paths.

Also, we observed the changes in current hysteresis with 5 cycles of voltage sweep (Figures S7 and S8, Supporting Information). The $CsPbBr_3$ PeLED with $CsBr:PbBr_2$ = 1:1 exhibited nearly negligible hysteresis from the second sweep. However, The $CsPbBr_3$ PeLED with $CsBr:PbBr_2$ = 1.5:1 exhibited large hysteresis until the fourth sweep and then negligible hysteresis at the fifth sweep. This indicates that nonstoichiometric amounts of precursors can facilitate the formation of charge traps.

Furthermore, to study ion migration, nonradiative pathways and electron–phonon interaction in the $CsPbBr_3$ PeLEDs, we used a nitrogen cryostat to measure PeLED characteristics at temperatures $80 \le T \le 300$ K. Current hysteresis occurred at all temperatures, and the hysteresis area A_{hys} increased exponentially until T = 280 K except for an anomalous point at 300 K (**Figure 4**a). The increase in A_{hys} was well-fitted by the following Arrhenius equation that has been used to describe temperature-dependence of ion migration[28,36–38,47]

$$A_{hys} = A_{hys,0} \exp\left(\frac{-E_{a,hys}}{k_B T}\right) \quad (1)$$

where $A_{hys,0}$ is a constant, $k_B = 8.617 \times 10^{-5}$ eV K^{-1} is the Boltzmann constant and T (K) is the temperature. Fitting with Equation (1) yielded the activation energy of hysteresis ($E_{a,hys}$) ≈ 90 ± 7 meV (r^2 = 0.985) (Table S1, Supporting Information), where the error is the standard error in the fitting. Current hysteresis in perovskite solar cells is closely related to ion migration,[28] so we posit that the current hysteresis in the PeLED originates from the creation of vacancies by ion migration. The calculated $E_{a,hys}$ ≈ 90 ± 7 meV can be linked to the activation energy E_a for migration of Br^- anions. This proposition can be supported by much lower E_a of halide anion migration than those of cation (e.g., MA^+ and Pb^{2+}) migrations in MHPs.[36–38,47] The reported E_a for halide anion migrations is 0.09 eV in $MAPbBr_3$,[36] 0.08–0.58 eV in $MAPbI_3$,[36–38] and 0.25 eV in $CsPbBr_3$.[39] E_a of MA^+ cation migration is ≈0.56 eV in $MAPbBr_3$[36] and 0.36–0.84 eV in $MAPbI_3$[36–38,40] which are larger than the E_a of halide anion migrations. E_a for Pb^{2+} cation migration is much larger than these: 0.8[36] or 2.31[38] eV in $MAPbI_3$. E_a of Cs^+ cation migration in $CsPbBr_3$ has not been reported yet, but it may be deduced to be larger than E_a of halide anion migration as in $MAPbBr_3$. Furthermore, the predominance of Br^- anion migration is supported by an experimental demonstration that $CsPbBr_3$ is a halide-ion conductor rather than a Cs^+-ion conductor.[39] Therefore, we conclude that current hysteresis in the $CsPbBr_3$ PeLED is related with Br^- anion migration.

The temperature dependence of the EL spectrum implies a change in the electronic structure of $CsPbBr_3$. As T increased, the EL spectrum area A_{EL} decreased (Figure 4c,d) in accordance with a modified Arrhenius equation[32–34]

$$A_{EL} = \frac{A_{EL,0}}{1 + B\exp\left(-E_{a,EL}/k_B T\right)} \quad (2)$$

where $A_{EL,0}$ is the EL spectrum area at 0 K. Fitting the data to Equation (2) yielded activation energy for an EL quenching channel $E_{a,EL}$ ≈ 41 ± 6 meV (Figure 4d ; Table S2, Supporting Information). This $E_{a,EL}$ may be related to both the exciton binding energy of $CsPbBr_3$ (35.0–54.7[32] or 40 meV[15,33] for $CsPbBr_3$ QDs) and the E_a of Br^- anion migration because luminescence quenching in MHPs can be caused by thermal activation of exciton dissociation,[32–34] and by trapping of charge carriers in thermally activated defects created by migration of halide anions.[29,31] Also, the difference between calculated values of $E_{a,EL}$ (41 ± 6 meV) and $E_{a,hys}$ (90 ± 7 meV) may indicate that EL quenching is not a result of Br^- ion migration alone, and that the contribution of exciton dissociation to EL quenching is not negligible.

The EL peak positions gradually blue-shifted with broadening of FWHM as T increased (Figure 4e,f). To understand

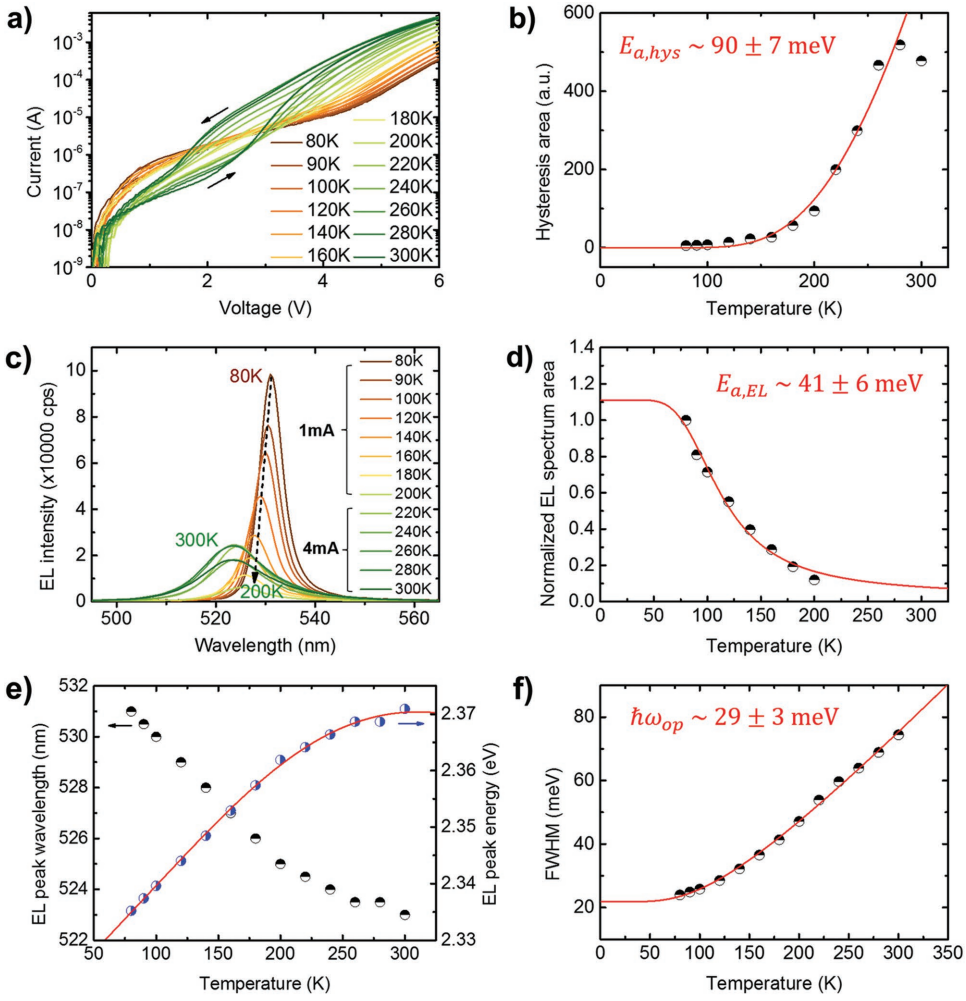

Figure 4. a) Temperature-dependent current–voltage characteristics of the $CsPbBr_3$ PeLED showing current hysteresis. b) Plot of hysteresis area versus T with a nonlinear fitting based on Arrhenius equation. The anomalous point at 300 K was excluded for the fitting. c) Temperature-dependence of EL spectrum in the $CsPbBr_3$ PeLED. Current source of 1 mA was applied at $80 \le T \le 200$ K and 4 mA was applied at $220 \le T \le 300$ K. d) Normalized EL spectrum area, e) EL peak wavelength (black) and energy (blue), and f) FWHM as a function of temperature.

the origins of blue-shift, EL peak energies that can be considered as bandgaps were fitted to[35]

$$E_g(T) = E_{g,0} + C_{th}T + C_{ep}\left(\frac{2}{\exp\left(\frac{\hbar\omega}{k_B T}\right) - 1} + 1\right) \quad (3)$$

where E_g (eV) is the bandgap, $E_{g,0}$ (eV) is the un-renormalized bandgap without thermal and phonon contributions, C_{th} (eV K^{-1}) is the coefficient regarding thermal expansion, C_{ep} (eV) is the coefficient regarding electron–phonon interaction, and $\hbar\omega$ (eV) is the average optical phonon energy. This equation is based on a one-oscillator model,[35] and explains the contributions of thermal expansion of lattice (second term) and electron–phonon interaction (third term) to the shift of bandgap. The fitting results (Table S3, Supporting Information) were excellent ($r^2 = 0.998$) and yielded $\hbar\omega \approx 105 \pm 15$ meV. The value of C_{ep} was negative; this result implies that the electron–phonon interaction decreases the bandgap. The fitting results suggest that the linear increase in EL peak energy at $80 \le T \le 200$ K is mainly attributable to thermal expansion, whereas the gradual decrease in slope at $T > 200$ K is a consequence of thermally activated electron–phonon interaction; this inference concords with a previous report.[35]

The linewidth broadening can be analyzed by fitting the plot to[32–35]

$$\Gamma(T) = \Gamma_0 + \Gamma_{ac}T + \frac{\Gamma_{op}}{\exp\left(\frac{\hbar\omega_{op}}{k_B T}\right) - 1} \quad (4)$$

where Γ (meV) is linewidth, Γ_0 (meV) is inhomogeneous broadening, $\hbar\omega_{op}$ (meV) is longitudinal optical phonon energy, Γ_{ac} (meV K^{-1}) is the contribution of exciton–acoustic phonon interaction, and Γ_{op} (meV) is the contribution of exciton–optical phonon interaction. The linewidth broadening by impurity scattering was neglected.[32–35] The fitting showed that the contribution of acoustic phonon is negligible and

that $\hbar\omega_{op} \approx 29 \pm 3$ meV (Table S4, Supporting Information), which is comparable to the reported optical phonon energies of $CsPbBr_3$ QDs (14.4–33.3 meV[32,35]). The difference between the optical phonon energies $\hbar\omega \approx 105 \pm 15$ meV obtained from the fitting of EL peak energy (Equation (3)) and $\hbar\omega_{op} \approx 29 \pm 3$ meV obtained from the fitting of EL linewidth (Equation (4)) can be understood by considering $\hbar\omega$ is an average value.

In conclusion, we have shown that $CsPbBr_3$ PeLEDs with high efficiency (5.39 cd A^{-1}) and high luminance (13752 cd m^{-2}) can be achieved by using uniform $CsPbBr_3$ polycrystalline layers fabricated by using 10.4 wt% $CsPbBr_3$ solutions and underlying Buf-HIL. XPS revealed the presence of PFI between $CsPbBr_3$ grains; this observation implies that PFI partially dissolved during spin-coating of $CsPbBr_3$ precursor solutions, which resulted in formation of uniform $CsPbBr_3$ layers on Buf-HIL because the PFI molecules impede $CsPbBr_3$ crystal growth or increase the number of nucleation sites.

Temperature-dependent current hysteresis in the $CsPbBr_3$ PeLED showed that the frequency of migration of Br^- anions increased exponentially with $E_{a,hys} = 90 \pm 7$ meV as T increased. The thermally activated EL quenching had an activation energy $E_{a,EL} = 41 \pm 6$ meV and could be explained by exciton dissociation and Br^- ion migration. Analysis of the spectral blue-shift revealed that the linear increase in bandgap at $T < 200$ K was mainly due to thermal expansion of lattice, and that the decrease in slope at $T > 200$ K was due to electron–phonon interaction. Broadening of the EL spectrum was well-explained by the interaction between excitons and longitudinal optical phonons with a phonon energy $\hbar\omega_{op} = 29 \pm 3$ meV. Our study has suggested simple and effective strategies to improve the brightness and efficiency of $CsPbBr_3$ PeLEDs and has shown the temperature dependence of ion migration and EL characteristics in $CsPbBr_3$ PeLEDs for the first time.

Although we achieved the high-efficiency polycrystalline $CsPbBr_3$ PeLEDs (EQE = 1.37%) which is much higher than those in previous works (0.008–0.15%),[18,27] the EQE is still lower than the efficiency of polycrystalline $MAPbBr_3$ PeLEDs (EQE = 8.53%).[2] To further improve the efficiency of polycrystalline $CsPbBr_3$ PeLEDs, the exciton binding energy should be increased and the Br^- ion migration should be suppressed. We expect that this work will stimulate studies of polycrystalline inorganic PeLEDs and related device physics.

Experimental Section

Preparation of $CsPbBr_3$ Solutions: $CsPbBr_3$ solutions (7.5, 9.0, and 10.4 wt%) were made by mixing CsBr (Aldrich) and $PbBr_2$ (Aldrich) ($CsBr:PbBr_2$ molar ratio = 2:1, 1.5:1, 1.2:1, 1.1:1, 1.05:1, 1:1, and 1:1.05) in DMSO at 60 °C while stirring vigorously. All solutions were cooled to room temperature before use.

Fabrication of $CsPbBr_3$ PeLEDs: $CsPbBr_3$ PeLEDs with structure of FTO/(Buf-HIL or PEDOT:PSS)/$CsPbBr_3$/TPBI/LiF/Al were fabricated and characterized using procedures previously reported.[2] The Buf-HIL[5] was used as a hole injection layer, and nanocrystal pinning[2] was not applied. The $CsPbBr_3$ layers were annealed at 70 °C for 10 min after spin-coating.

XPS and UPS Measurement: XPS and UPS measurement of ITO/Buf-HIL/$CsPbBr_3$ samples were conducted as in the previous work,[2] using the same equipment in collaboration with Korea Basic Science Institute (KBSI).

Temperature-Dependent PeLED Characterization: Temperature-dependent characterization of $CsPbBr_3$ PeLEDs was conducted using an N_2 cryostat (OptistatDN2, Oxford Instruments) in N_2 atmosphere. Temperature was controlled by a custom-made program and a cryogenic environment controller (Mercury iTC, Oxford Instruments); measurements were taken after temperature stabilization for 1 min. The sample temperatures are believed to be accurate within 1 K of the sensor read-out, according to manufacturer specifications. For biasing the devices, a constant current level was set using a Keysight B1500A semiconductor parameter analyzer and the EL spectrum was monitored through a fiber-coupled StellarNet BLUE-Wave spectrometer.

Supporting Information

Supporting Information is available from the Wiley Online Library or from the author.

Acknowledgements

This work was supported by the National Research Foundation of Korea (NRF) grant funded by the Korea government (Ministry of Science, ICT & Future Planning) (NRF-2016R1A3B1908431). All data are available in the main text and the Supporting Information.

Conflict of Interest

The authors declare no conflict of interest.

Keywords

cesium lead halides, electron–phonon coupling, inorganic halide perovskites, light-emitting diodes, next-generation emitters

Received: January 28, 2017
Revised: April 30, 2017
Published online: June 13, 2017

[1] a) Y.-H. Kim, H. Cho, T.-W. Lee, *Proc. Natl. Acad. Sci. U S A* **2016**, *113*, 11694; b) Z.-K. Tan, R. S. Moghaddam, M. L. Lai, P. Docampo, R. Higler, F. Deschler, M. Price, A. Sadhanala, L. M. Pazos, D. Credgington, F. Hanusch, T. Bein, H. J. Snaith, R. H. Friend, *Nat. Nanotechnol.* **2014**, *9*, 687.
[2] H. Cho, S.-H. Jeong, M.-H. Park, Y.-H. Kim, C. Wolf, C.-L. Lee, J. H. Heo, A. Sadhanala, N. Myoung, S. Yoo, S. H. Im, R. H. Friend, T.-W. Lee, *Science* **2015**, *350*, 1222.
[3] N. J. Jeon, J. H. Noh, W. S. Yang, Y. C. Kim, S. Ryu, J. Seo, S. Il Seok, *Nature* **2014**, *517*, 476.
[4] H. Kim, K.-G. Lim, T.-W. Lee, *Energy Environ. Sci.* **2016**, *9*, 12.
[5] Y.-H. Kim, H. Cho, J. H. Heo, T.-S. Kim, N. Myoung, C.-L. Lee, S. H. Im, T.-W. Lee, *Adv. Mater.* **2015**, *27*, 1248.
[6] a) H.-K. Seo, H. Kim, J. Lee, M.-H. Park, S.-H. Jeong, Y.-H. Kim, S.-J. Kwon, T.-H. Han, S. Yoo, T.-W. Lee, *Adv. Mater.* **2017**, *29*, 1605587; b) Y.-H. Kim, G.-H. Lee, Y.-T. Kim, C. Wolf, H. J. Yun, W. Kwon, C. G. Park, T.-W. Lee, *Nano Energy* **2017**, *38*, 51.
[7] J. Byun, H. Cho, C. Wolf, M. Jang, A. Sadhanala, R. H. Friend, H. Yang, T.-W. Lee, *Adv. Mater.* **2016**, *28*, 7515.

[8] J. C. Yu, D. B. Kim, G. Baek, B. R. Lee, E. D. Jung, S. Lee, *Adv. Mater.* **2015**, *27*, 3492.
[9] Y. K. Chih, J. C. Wang, R. T. Yang, C. C. Liu, Y. C. Chang, Y. S. Fu, W. C. Lai, P. Chen, T. C. Wen, Y. C. Huang, C. S. Tsao, T. F. Guo, *Adv. Mater.* **2016**, *28*, 8687.
[10] J. C. Yu, D. B. Kim, E. D. Jung, B. R. Kim, M. H. Song, *Nanoscale* **2016**, *8*, 7036.
[11] J. C. Yu, D. W. Kim, D. B. Kim, E. D. Jung, K.-S. Lee, S. Lee, D. Di Nuzzo, J.-S. Kim, M. H. Song, *Nanoscale* **2017**, *9*, 2088.
[12] M. Yuan, L. N. Quan, R. Comin, G. Walters, R. Sabatini, O. Voznyy, S. Hoogland, Y. Zhao, E. M. Beauregard, P. Kanjanaboos, Z. Lu, D. H. Kim, E. H. Sargent, *Nat. Nanotechnol.* **2016**, *11*, 872.
[13] N. Wang, L. Cheng, R. Ge, S. Zhang, Y. Miao, W. Zou, C. Yi, Y. Sun, Y. Cao, R. Yang, Y. Wei, Q. Guo, Y. Ke, M. Yu, Y. Jin, Y. Liu, Q. Ding, D. Di, L. Yang, G. Xing, H. Tian, C. Jin, F. Gao, R. H. Friend, J. Wang, W. Huang, *Nat. Photonics* **2016**, *10*, 699.
[14] X. Zhao, N.-G. Park, *Photonics* **2015**, *2*, 1139.
[15] L. Protesescu, S. Yakunin, M. I. Bodnarchuk, F. Krieg, R. Caputo, C. H. Hendon, R. X. Yang, A. Walsh, M. V. Kovalenko, *Nano Lett.* **2015**, *15*, 3692.
[16] M. Kulbak, S. Gupta, N. Kedem, I. Levine, T. Bendikov, G. Hodes, D. Cahen, *J. Phys. Chem. Lett.* **2016**, *7*, 167.
[17] A. Swarnkar, R. Chulliyil, V. K. Ravi, M. Irfanullah, A. Chowdhury, A. Nag, *Angew. Chem., Int. Ed.* **2015**, *54*, 15424.
[18] N. Yantara, S. Bhaumik, F. Yan, D. Sabba, H. A. Dewi, N. Mathews, P. P. Boix, H. V. Demir, S. Mhaisalkar, *J. Phys. Chem. Lett.* **2015**, *6*, 4360.
[19] J. Song, J. Li, X. Li, L. Xu, Y. Dong, H. Zeng, *Adv. Mater.* **2015**, *27*, 7162.
[20] X. Zhang, H. Lin, H. Huang, C. Reckmeier, Y. Zhang, W. C. H. Choy, A. L. Rogach, *Nano Lett.* **2016**, *16*, 1415.
[21] G. Li, F. W. R. Rivarola, N. J. L. K. Davis, S. Bai, T. C. Jellicoe, F. De La Peña, S. Hou, C. Ducati, F. Gao, R. H. Friend, N. C. Greenham, Z. K. Tan, *Adv. Mater.* **2016**, *28*, 3528.
[22] X. Zhang, B. Xu, J. Zhang, Y. Gao, Y. Zheng, K. Wang, X. W. Sun, *Adv. Funct. Mater.* **2016**, *26*, 4595.
[23] J. Pan, L. N. Quan, Y. Zhao, W. Peng, B. Murali, S. P. Sarmah, M. Yuan, L. Sinatra, N. M. Alyami, J. Liu, E. Yassitepe, Z. Yang, O. Voznyy, R. Comin, M. N. Hedhili, O. F. Mohammed, Z. H. Lu, D. H. Kim, E. H. Sargent, O. M. Bakr, *Adv. Mater.* **2016**, *28*, 8718.
[24] H. Huang, H. Lin, S. V. Kershaw, A. S. Susha, W. C. H. Choy, A. L. Rogach, *J. Phys. Chem. Lett.* **2016**, *7*, 4398.
[25] X. Zhang, C. Sun, Y. Zhang, H. Wu, C. Ji, Y. Chuai, P. Wang, S. Wen, C. Zhang, W. W. Yu, *J. Phys. Chem. Lett.* **2016**, *7*, 4602.
[26] Y. Ling, Y. Tian, X. Wang, J. C. Wang, J. M. Knox, F. Perez-Orive, Y. Du, L. Tan, K. Hanson, B. Ma, H. Gao, *Adv. Mater.* **2016**, *28*, 8983.
[27] Z. Wei, A. Perumal, R. Su, S. Sushant, J. Xing, Q. Zhang, S. T. Tan, H. V. Demir, Q. Xiong, *Nanoscale* **2016**, *8*, 18021.
[28] Y. Shao, Y. Fang, T. Li, Q. Wang, Q. Dong, Y. Deng, Y. Yuan, H. Wei, M. Wang, A. Gruverman, J. Shield, J. Huang, *Energy Environ. Sci.* **2016**, *9*, 1752.
[29] Y. Tian, M. Peter, E. Unger, M. Abdellah, K. Zheng, T. Pullerits, A. Yartsev, V. Sundström, I. G. Scheblykin, *Phys. Chem. Chem. Phys.* **2015**, *17*, 24978.
[30] X. Wen, A. Ho-Baillie, S. Huang, R. Sheng, S. Chen, H. C. Ko, M. A. Green, *Nano Lett.* **2015**, *15*, 4644.
[31] S. Chen, X. Wen, R. Sheng, S. Huang, X. Deng, M. A. Green, A. Ho-Baillie, *ACS Appl. Mater. Interfaces* **2016**, *8*, 5351.
[32] J. Li, X. Yuan, P. Jing, J. Li, M. Wei, J. Hua, J. Zhao, L. Tian, *RSC Adv.* **2016**, *6*, 78311.
[33] X. Li, Y. Wu, S. Zhang, B. Cai, Y. Gu, J. Song, H. Zeng, *Adv. Funct. Mater.* **2016**, *26*, 2435.
[34] K. Wu, A. Bera, C. Ma, Y. Du, Y. Yang, L. Li, T. Wu, *Phys. Chem. Chem. Phys.* **2014**, *16*, 22476.
[35] K. Wei, Z. Xu, R. Chen, X. Zheng, X. Cheng, T. Jiang, *Opt. Lett.* **2016**, *41*, 3821.
[36] J. M. Azpiroz, E. Mosconi, J. Bisquert, F. De Angelis, *Energy Environ. Sci.* **2015**, *8*, 2118.
[37] J. Haruyama, K. Sodeyama, L. Han, Y. Tateyama, *J. Am. Chem. Soc.* **2015**, *137*, 10048.
[38] C. Eames, J. M. Frost, P. R. F. Barnes, B. C. O'Regan, A. Walsh, M. S. Islam, *Nat. Commun.* **2015**, *6*, 7497.
[39] J. Mizusaki, K. Arai, K. Fueki, *Solid State Ionics* **1983**, *11*, 203.
[40] Y. Yuan, J. Chae, Y. Shao, Q. Wang, Z. Xiao, A. Centrone, J. Huang, *Adv. Energy Mater.* **2015**, *5*, 1500615.
[41] D. Bi, C. Yi, J. Luo, J.-D. Décoppet, F. Zhang, S. M. Zakeeruddin, X. Li, A. Hagfeldt, M. Grätzel, *Nat. Energy* **2016**, *1*, 16142.
[42] C. C. Stoumpos, C. D. Malliakas, J. A. Peters, Z. Liu, M. Sebastian, J. Im, T. C. Chasapis, A. C. Wibowo, D. Y. Chung, A. J. Freeman, B. W. Wessels, M. G. Kanatzidis, *Cryst. Growth Des.* **2013**, *13*, 2722.
[43] J. F. Moulder, W. F. Stickle, P. E. Sobol, K. D. Bomben, *Handbook of X-Ray Photoelectron Spectroscopy*, Perkin-Elmer Corporation, Eden Prairie, MN, USA, **1992**.
[44] E. A. Hoffmann, Z. A. Fekete, L. S. Korugic-Karasz, F. E. Karasz, E. Wilusz, *J. Polym. Sci., Part A: Polym. Chem.* **2004**, *42*, 551.
[45] T. W. Lee, Y. Chung, O. Kwon, J. J. Park, *Adv. Funct. Mater.* **2007**, *17*, 390.
[46] T.-H. Han, Y. Lee, M.-R. Choi, S.-H. Woo, S.-H. Bae, B. H. Hong, J.-H. Ahn, T.-W. Lee, *Nat. Photonics* **2012**, *6*, 105.
[47] Y. Yuan, J. Huang, *Acc. Chem. Res.* **2016**, *49*, 286.

